Separation Science and Technology
Publication details, including instructions for authors and subscription information:
http://www.informaworld.com/smpp/title~content=t713708471

Separation of Inorganic Salts From Supercritical Water by Cross-Flow Microfiltration

M. G. E. Goemans[a]; L. Li[a]; E. F. Gloyna[a]
[a] Environmental and Water Resources Engineering, and Separations Research Program, The University of Texas at Austin, Austin, Texas

To cite this Article Goemans, M. G. E. , Li, L. and Gloyna, E. F.(1995) 'Separation of Inorganic Salts From Supercritical Water by Cross-Flow Microfiltration', Separation Science and Technology, 30: 7, 1491 — 1509
To link to this Article: DOI: 10.1080/01496399508010359
URL: http://dx.doi.org/10.1080/01496399508010359

SEPARATION SCIENCE AND TECHNOLOGY, 30(7-9), pp. 1491-1509, 1995

SEPARATION OF INORGANIC SALTS FROM SUPERCRITICAL WATER BY CROSS-FLOW MICROFILTRATION

M. G. E. Goemans, L. Li, and E. F. Gloyna
Environmental and Water Resources Engineering, and
Separations Research Program
The University of Texas at Austin
Austin, Texas 78712

ABSTRACT

A cross-flow microfilter capable of operating at elevated temperatures and pressures was evaluated for its ability to remove inorganic salts from supercritical water (SCW). The separation characteristics of molten sodium nitrate were investigated. The overall performance of the cross-flow microfilter and the effects of process variables on the separation efficiency were evaluated. Separation efficiencies up to 85% were observed. An empirical model was developed for the prediction of the filtrate salt concentration and the fluidized cake resistance as a function of the salt solubility and salt flux to the filter. Physical principles governing the separation process were defined.

INTRODUCTION

The supercritical water oxidation (SCWO) process is an effective treatment technology for many organic wastewaters and sludges. In the SCWO process, organic matter is oxidized in water above its critical point (374.2°C, 22.1 MPa). High destruction efficiencies at relatively short residence times are obtained (1,2).

The unique feature of supercritical water (SCW) is the drastic change in physico-chemical properties near its critical region. At typical SCWO conditions (450°C, 27.6 MPa), the density and viscosity are reduced to 128 kg/m^3 and 0.3 10^{-4} Pa.s respectively (3). These reductions result in changed mass-transfer

characteristics, with Brownian diffusion 40 times greater in SCW than in water at ambient conditions (4). In addition, the dielectric constant is reduced below ten (5), the ion product is decreased below 10^{-21}, and the extent of hydrogen bonding is significantly reduced. The drastic change in these physico-chemical properties results in increased solubility of organic components (6) and gases (7) and decreased solubility of electrolytes (8,9).

Inorganic salts may be generated during SCWO of wastewaters. The presence of these salts may cause corrosion, erosion, and fouling of equipment. Therefore, the efficiency of reactors, heat exchangers, and pressure reduction devices may be impaired. In addition, salt removal from the effluent might be desired for regulatory reasons. A solution to the salt problem is to remove the insoluble salt fraction within the supercritical region. The separation of salts from supercritical water is physically favorable because the solubility of inorganic salts in supercritical water is low, the viscous forces holding salt crystals in suspension are low, and the density differential between the insoluble salt phase and the water phase is large.

Limited data exist describing solid-fluid separation under high pressure and temperature conditions. Killilea et al. (10) studied microgravity and impingement/filtration as possible methods for removing metal oxide particles from supercritical water. Dell'Orco et al. (11) reported cyclone removal efficiencies up to 99% for micron-sized silica, zirconium oxide, and titanium oxide particles. Engineering designs equations were developed. Salt separation using cyclones was shown to be poor (10) due to the stickiness of the salts to the cyclone walls. Armellini and Tester (12) studied salt nucleation phenomena in supercritical water and reported sodium chloride solubilities in water at supercritical conditions (13). Dell'Orco et al. (14) studied removal mechanisms for sodium salts in a settling vessel at SCW conditions. Sodium chloride, sodium sulfate, and sodium carbonate/bicarbonate appeared to be removed by impingement on reactor walls, while sodium nitrate appeared to be removed by settling. To date, salt-fluid separation studies conducted at SCWO conditions did not yield conclusive engineering design data for inorganic salt/SCW separation devices.

The objective of this research was to obtain engineering design data for a cross-flow microfiltration device capable of removing inorganic salts from water

at elevated temperatures and pressures. Sodium nitrate was chosen to be studied because its solubility under the experimental conditions was known (14). Under SCW conditions, sodium nitrate is present in a molten state (melting point = 306.8°C). The molten condition of sodium nitrate makes it a good example for other salts with melting points below the critical point, such as sodium nitrite, sodium hydroxide, sodium bicarbonate, magnesium hydroxide, aluminum nitrate, and aluminum hydroxide. These salts are commonly present in SCWO process effluents.

EXPERIMENTAL

The separation apparatus (Figure 1) was incorporated into a 150-L/h SCWO pilot plant (Figure 2). Table 1 shows the filter element and filter housing characteristics. The sodium nitrate solution was pressurized with a high-pressure diaphragm pump. After passing through a mass flow meter, the pressurized feed stream was preheated by two 6.6-m-long tube and shell heat exchangers. Heating to the desired temperature was accomplished with a tubular 6.6-m-long heater. After exiting the heat exchanger, the solution entered the cross-flow microfilter (Figure 2). Differential pressure over the filter element was measured with a differential pressure transducer. The fluid temperature was measured at the heater outlet, filter inlet, filtrate outlet, and the retentate outlet with Inconel-sheathed, type-K thermocouples. Fluid temperatures in the filter were estimated by surface temperatures of the filter housing. Surface temperatures were 3.6% lower than fluid temperatures on average (4). The filtrate stream was cooled by heat exchange with the feed and by an additional chilled water heat exchanger. Prior to entering a pneumatically controlled pressure reduction valve, the filtrate flowed through a three-way ball valve, which was part of the backflush equipment. The filtrate flow was measured with a mass flow meter prior to effluent collection. The collected filtrate was weighted (for flow rate verification) and sampled at 15- to 20-min intervals.

The retentate stream was cooled to ambient temperatures by a chilled water heat exchanger prior to passing through a manually controlled pressure reducing valve. Retentate was collected, measured, and analyzed. At the end of the

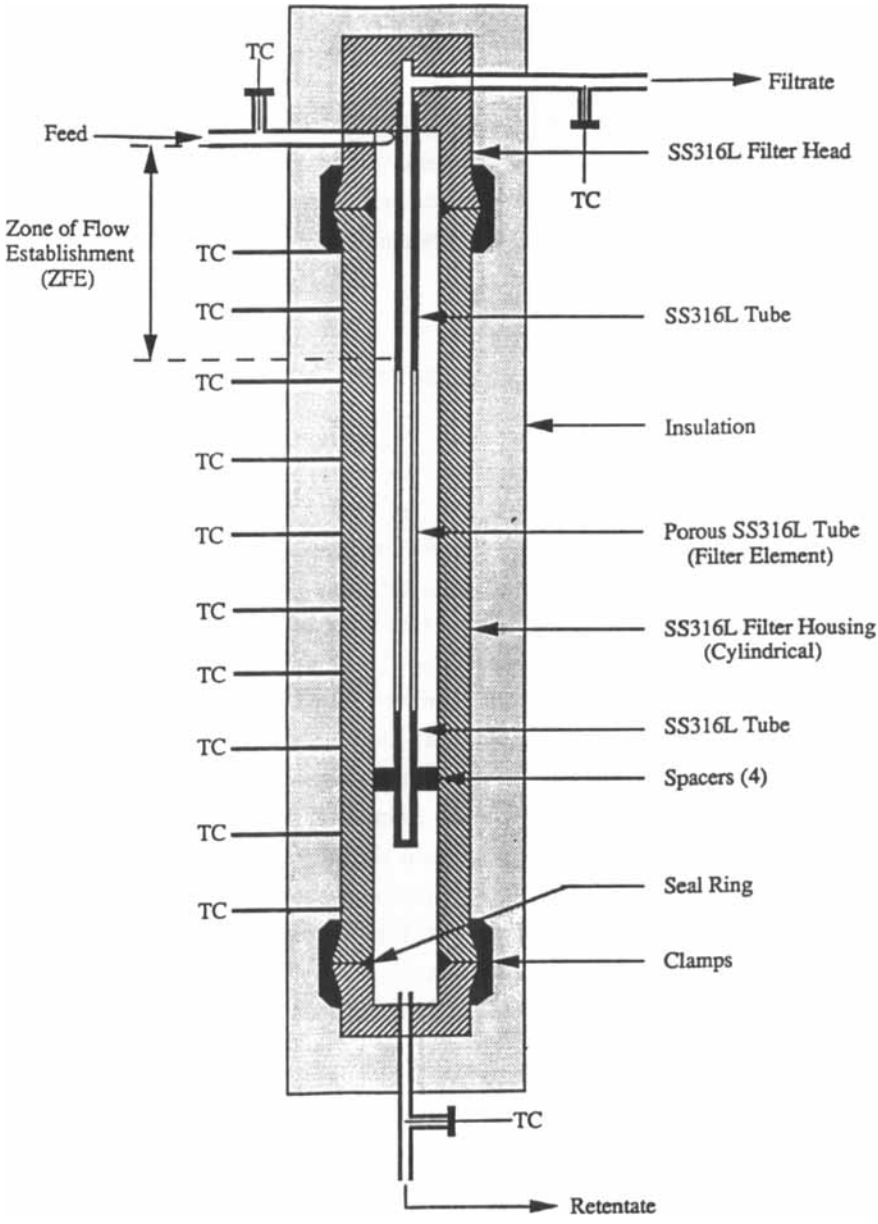

FIGURE 1. Cross-flow microfilter.

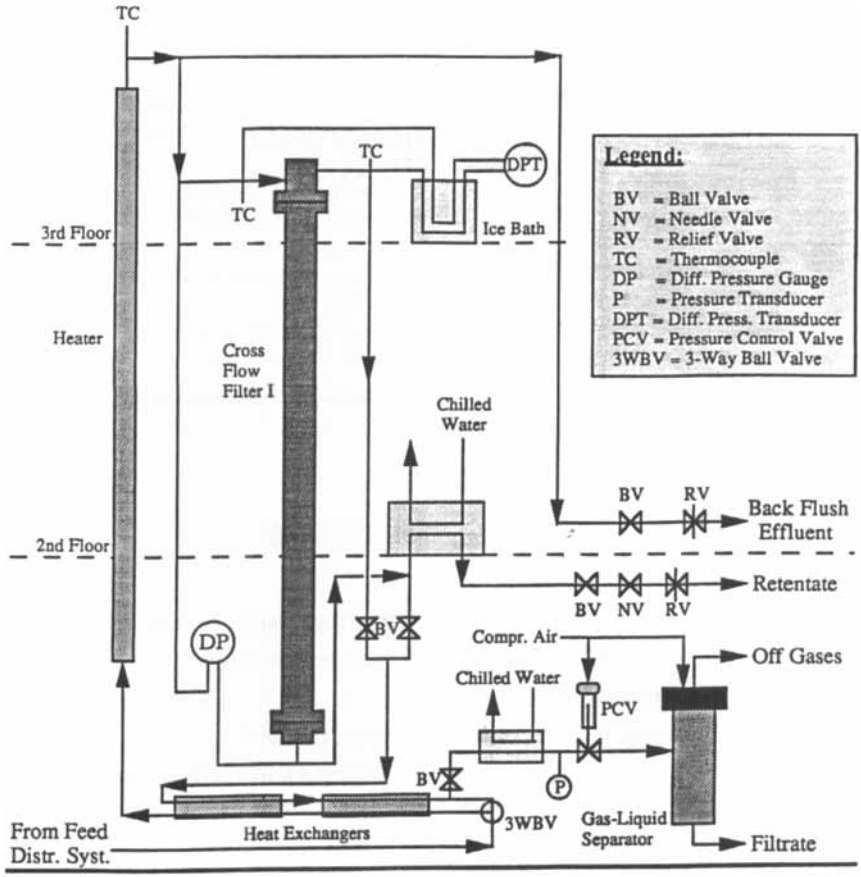

FIGURE 2. Salt separation apparatus.

experiment, the system temperature was reduced below the critical point of water to resolubilize sodium nitrate deposits in the filter pores and equipment walls. Rinse water was collected, weighted, and analyzed.

Feed, filtrate, and retentate samples were collected for all experiments. Each sample was representative for a known volume of effluent. Effluent volumes were measured by weight (filtrate) or by graduated cylinder (retentate). Samples were analyzed for pH, chloride, nitrate, nitrite, sodium, and chromium. Anions were analyzed by ion chromatography (IC) and cations were analyzed by ion coupled plasma emission spectroscopy (ICP).

TABLE 1. DESIGN CHARACTERISTICS OF FILTER ELEMENT AND FILTER HOUSING.

Filter Housing		Filter Element	
Construction Material	SS316L	Construction Material	SS316L
Length (m)	6.10	Length (m)	2.1
Inner Diameter (mm)	50.80	Inner Diameter (mm)	19.05
Outer Diameter (mm)	88.90	Outer Diameter (mm)	25.40
Geometry	Tubular	Geometry	Tubular
Design Temperature (°C)	590	Surface Area (cm^2)	1700
Design Pressure (MPa)	34.5	Pore Size (μm)	0.5
Number of Fluid TCs	3	Max. Filtr. Flux ($kg/s.m^2$)	0.41
Number of Surface TCs	10	Bubble Pressure (kPa)	10.1-13.1
Surface TC Interval (m)	0.61	Length Extension Tube (m)	1.0

RESULTS AND DISCUSSION

Table 2 shows operating conditions for salt separation studies. Experiments were conducted at 27.6 MPa and temperatures ranging from 400°C to 470°C. Feed concentrations ranged from 4,770 mg/kg to 22,500 mg/kg (sodium nitrate, A.C.S. Reagent, crystals, Aldrich or EMScience), feed flow rates ranged from 63 kg/h to 111 kg/h, and filtrate flow rates were 80% to 100% of the feed flow rates. This implied that the cross-flow filter was operated as a semicartridge filter with a continuous collection of the retentate from the bottom of the filter. The fluid residence time in the filter ranged from 45 to 60 s.

Mass flow rates were converted into bulk fluid velocities (V_b), filtrate fluxes (V_w), and shear rates along the filter (γ_w) to evaluate the effect of different process parameters on the filtrate concentration and filter cake properties. The solution densities and viscosities were approximated by steam table data (3,15). The evaluation of filter performance was based on the impact of process parameters on the filtrate concentration.

Calculation of Fluid Dynamic Properties in the Filter

The experimental values for the bulk fluid velocity at the filter inlet (V_{bo}); the average filtrate flux (V_{wav}); the minimum, maximum, and average shear rate (γ_{wmin}, γ_{wmax}, γ_{wav}); and the minimum and maximum Reynolds numbers (Re_{min},

TABLE 2. SODIUM NITRATE SEPARATION EXPERIMENTS
(P = 27.6 MPA)

Experiment ID#	Feed Concentration (mg/kg)	Temperature Range* (°C)	Feed Mass Flow Rate** (kg/h)	Filtrate Mass Flow Rate** (kg/h)
2-1	5,150	422-445	73	65
2-2	4,770	455-470	70	63
2-3	4,970	401-402	96	86
2-4	4,830	434-444	93	84
2-5A	5,150	435-446	94	75
2-5B	5,150	435-446	94	94
2-6	5,150	428-439	113	102
2-7	10,900	423-438	65	61
2-8	14,000	423-438	63	57
2-9	19,600	425-439	63	57
2-10	21,300	430-442	73	65
2-11	21,300	403-404	97	87
2-12	21,300	431-439	95	85
2-13	22,500	384-424	111	100

* Temperature measured at exterior of filter housing. The minimum and maximum temperature observed during the experiment are reported.
** Mass flow rates are ± 5%.
*** Filter was operated as a cartridge filter during exp. 2-5B.

Re_{max}) are presented in Table 3. The initial feed velocity (V_{bo}), average filtrate flux (V_{wav}), and average retentate velocity (V_{br}) were coupled through the conservation balance $Q_{feed} = Q_{filtrate} + Q_{retentate}$, resulting in Eq. 1:

$$V_{bo}*\rho_{scw}*A_a = V_{wav}*\rho_{scw}*A_f + V_{br}*\rho_{scw}*A_a, \quad (1)$$

where

A_a = cross-section between filter element and housing (m^2),
A_f = external area of the filter element (m^2),
Q = mass flow rate (kg/s),
ρ_{scw} = average supercritical water density (kg/m^3), calculated using the average temperature along the filter.

The initial average bulk velocity (V_{bo}) was defined as the average fluid velocity at the end of the zone of flow establishment (ZFE), shown in Figure 1. Due to equipment limitations it was impossible to determine the filtrate flux

TABLE 3. FLOW CHARACTERISTICS IN THE CROSS-FLOW FILTER DURING SALT SEPARATION EXPERIMENTS

Exp. ID#	V_{bo} (m/s)	V_{wav} (10^{-4} m/s)	γ_{wmax} (s^{-1})	γ_{wmin} (s^{-1})	γ_{wav} (s^{-1})	Re_{max}	Re_{min}
2-1	0.101	7.92	28.9	1.45	16.6	10,800	543
2-2	0.111	8.93	33.2	2.22	19.9	10,700	713
2-3	0.077	5.45	21.7	2.79	15.0	12,000	1,540
2-4	0.128	10.6	38.9	2.12	22.6	14,600	799
2-5A	0.131	9.39	40.4	7.81	31.9	14,700	2,840
2-5B	0.131	10.5	36.7	0.00	18.3	13,500	0
2-6	0.150	11.8	44.9	3.79	28.1	17,600	1,490
2-7	0.086	7.06	25.9	1.45	15.2	10,200	572
2-8	0.083	6.44	24.7	2.32	15.8	9,780	921
2-9	0.083	6.28	24.0	2.15	15.2	9,460	848
2-10	0.099	7.50	27.7	1.71	16.4	10,700	660
2-11	0.083	6.50	25.2	2.67	16.6	13,600	1,440
2-12	0.126	9.84	36.8	2.64	22.4	14,300	1,020
2-13	0.130	9.53	37.7	4.65	25.8	16,500	2,040

profile along the filter. Therefore, the average filtrate flux was defined as the ratio of the observed filtrate mass flow rate over the area of the filter element. The minimum and maximum shear rates and Reynolds numbers were calculated using the average minimum and maximum bulk fluid velocity respectively ($V_{bmax} = V_{bo}$, $V_{bmin} = V_{br}$). The shear rates were calculated according to Cheryan (16) and Henry (17). Quantification of the shear rate assessed the strength of the shear stress on the salt layer that was formed on the filter element. The average shear rates obtained during the salt separation experiments were typical for low shear cross-flow filtration applications (18).

Assuming a linear decrease in the bulk fluid velocity, it was estimated that turbulent flow existed along 80 to 90% of the filter element. Because transition from laminar to turbulent flow occurs at a Reynolds number less than 2000 (19) for tubes with porous walls, turbulent flow probably extended along the entire filter, except for exp. 2-5B.

Results of IC and ICP Analysis

Experimental results are shown in Table 4. Mass balances for sodium nitrate ranged from 82 to 126%. Unrecovered mass was accounted for by two

TABLE 4. EXPERIMENTAL RESULTS FOR THE SEPARATION EXPERIMENTS

Exp. ID#	Filtrate Conc. (mg/kg)	Separation Efficiency (%)	Mass Balance (%)	pH Feed	pH Retent.	pH Filtrate
2-1	836 (174)	84.6 (3.19)	95.6	9.3	10.3	3.5
2-2	818 (266)	84.0 (5.19)	94.2	9.7	10.9	4.4
2-3	3410 (297)	40.5 (4.79)	116	6.9	7.0	4.2
2-4	1180 (157)	76.8 (3.21)	85.3	9.8	11.1	3.9
2-5A	1070 (291)	83.1 (5.08)	103	9.3	6.0	3.1
2-5B	1460 (72.5)	71.7 (1.41)	103	9.3	------	3.1
2-6	1250 (294)	78.0 (4.68)	82.4	9.3	9.0	3.5
2-7	2130 (168)	81.6 (1.49)	115	4.9	11.2	3.8
2-8	3730 (1210)	71.5 (7.81)	123	8.3	10.7	3.4
2-9	6140 (1640)	68.7 (2.58)	116	6.0	10.8	4.2
2-10	7031 (1470)	69.2 (6.05)	106	9.6	10.6	3.3
2-11	7810 (1380)	65.2 (3.42)	121	9.6	9.8	3.8
2-12	9030 (1060)	60.7 (4.69)	119	9.6	9.0	3.3
2-13	8550 (2770)	62.2 (3.05)	96.6	9.3	7.4	3.5

* Values in parentheses are the standard deviations
** Concentrations and separation efficiencies are the average of 2 to 6 values

mechanisms: (a) sodium precipitated with corrosion products, primarily chromate, that was retained in the apparatus prior to rinsing; and (b) molten sodium nitrate that precipitated in dead ended connecting tubes. Operational limitations accounted for the surplus in mass. Collection of the rinse water was started at the same time the feed was switched from the sodium nitrate solution to water. However, a certain amount of residual sodium nitrate solution remained in the system. The amount of residual mass was a function of volume, fluid density, and

feed concentration: hence, the residual mass was estimated by adding the product of these three parameters for the different temperature zones in the SCWO system.

Separation efficiencies (E), defined as $E = 100*(1-C_{filtrate}/C_{feed})$, were 60% and 85% for experiments conducted at 420°C and 470°C, respectively. Separation efficiency decreased to about 40% at 400°C, while filtrate concentrations increased with increasing feed concentrations. Increasing filtrate and retentate concentrations with time indicated salt accumulation in the cross-flow filter. Times required to establish constant salt concentrations in the filtrate and retentate streams increased from 20 to 100 min with increasing feed concentration and filtrate flux.

Changes in the pH of filtrate and retentate were observed during the cross-flow filtration of a sodium nitrate solution. The pH of the feed solution was typically near 9. The filtrate pH ranged from 3.1 to 4.2, while the pH of the retentate ranged from 9.0 to 11.2. The formation of hexavalent chromium and nitrite indicated that electrochemical corrosion of the filter element was the predominant mechanism responsible for the observed pH phenomena (4).

Solubility effects were observed when feed solutions containing 4770 to 5150 mg/kg sodium nitrate were filtered. Sodium nitrate solubilities were estimated using an empirical equation developed by Dell'Orco et al. (14). This equation showed a strong dependence on the fluid density (Eq. 2):

$$\log_e(S) = 13.396 + 3.166 * \log_e(\rho_{scw}), \quad (2)$$

where ρ_{scw} is the density of supercritical water (g/cc) and S the sodium nitrate solubility in mg/kg. The deviation between the predicted salt solubility and the observed filtrate concentration increased with increased feed concentration, increased filtrate flux, and increased feed mass flow rates (Table 4). The maximum achievable salt separation was limited by the salt solubility limit for the given process temperature and pressure, as shown by Figure 3 (4).

To eliminate the influences of the filter configuration on the separation efficiency, the filtrate concentration was expressed as a function of the salt flux onto the filter. The salt flux variable was a combination of the feed concentration,

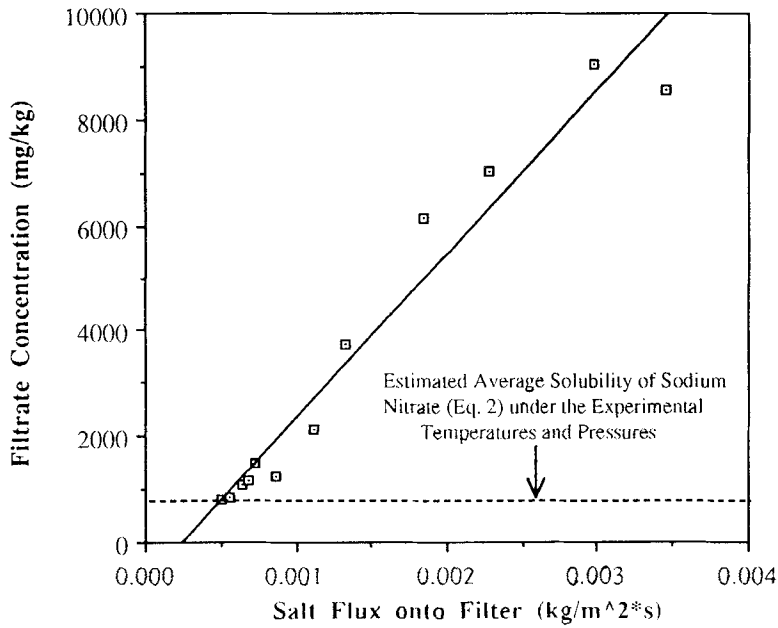

FIGURE 3. Correlation between the filtrate concentration and total salt flux to the filter (P = 27.6±0.7 MPa; T = 420-450°C).

filtrate mass flow rate, and area of the filter. This salt flux was defined by Eq. 3:

$$J_{salt} = \frac{Q_{filtrate} * C_{feed}}{A_{filter}}, \tag{3}$$

where the salt flux (J_{salt}) was expressed in kg/m^{2}s. Salt fluxes ranged from 5.07 kg/m^{2}s to 34.5 kg/m^{2}s. Another important feature of the salt flux is the independence of the fluid density. Figure 3 shows the correlation between the filtrate concentration and the salt flux onto the filter. The filtrate concentration was regressed with the salt flux for all experiments conducted in the 420°C to 450°C temperature range. This resulted in an empirical expression for predicting the filtrate salt concentration:

$$C_{filtr} = -7.877*10^{+2} + 3.104*10^{+6}\,(J_{salt})\,. \tag{4}$$

The R^2 value for this regression was 0.954, and the p-value for the F-test was 0.0001. In addition, the insoluble fraction of the feed and filtrate concentration was calculated by subtracting the salt solubility (Eq. 2) from the total feed and filtrate concentration. The insoluble fraction of the filtrate concentration (C^*_{filtr}) was then correlated with the insoluble fraction of the salt flux (J^*_{salt}). The regression equation was $C^*_{filtr} = -7.524*10^{+2} + 2.737*10^{+6}\ (J^*_{salt})$ with $R^2 = 0.930$.

Filtration Characteristics

The transmembrane pressure drop and filtrate mass flow rate were measured over time for all salt separation experiments. Medium, cake, and total resistances were calculated. The transient membrane, cake, and total resistance trends shown in Figure 4 were representative for all salt separation experiments. The membrane resistance was calculated by Darcy's equation, $R_m = \Delta P/\mu V_w$, where V_w was the transient average filtrate flux and ΔP the observed initial pressure drop across the clean filter. This method for calculating the medium resistance was valid because back flushing was not required during any of experiments and because the pressure drop decreased to its initial value when the feed was switched back to water at the end of the experiment. The total resistance was calculated using Darcy's equation where the pressure drop was the observed transient pressure drop during filtration of the salt solution. The cake resistance was defined as the difference between the total resistance and medium resistance. The resistance profiles as shown in Figure 4 were typical for cross-flow filtration with no membrane fouling and gradual filter cake buildup. A fluidized filter cake was believed to exist because of the molten condition of the salt. Steady state conditions were established 40 min after the experiment was started. Minor fluctuations of the cake resistance after "steady state" was achieved were attributed to erratic pulsation dampening and leakage of the check valves of the feed pump. Steady state transmembrane pressure drop ranged from 140 KPa for exps. 2-1 through 2-6 and increased to about 220 KPa for exp. 2-9.

Figures 5 and 6 show the effect of the shear rate on the steady state cake resistance. A higher shear rate resulted in a lower cake resistance, which was in agreement with earlier research about cross-flow filtration of particle suspensions at ambient conditions (20, 21). The effect of the salt flux on the cake resistance is shown in Figure 7. A linear increase of the steady state cake resistance with

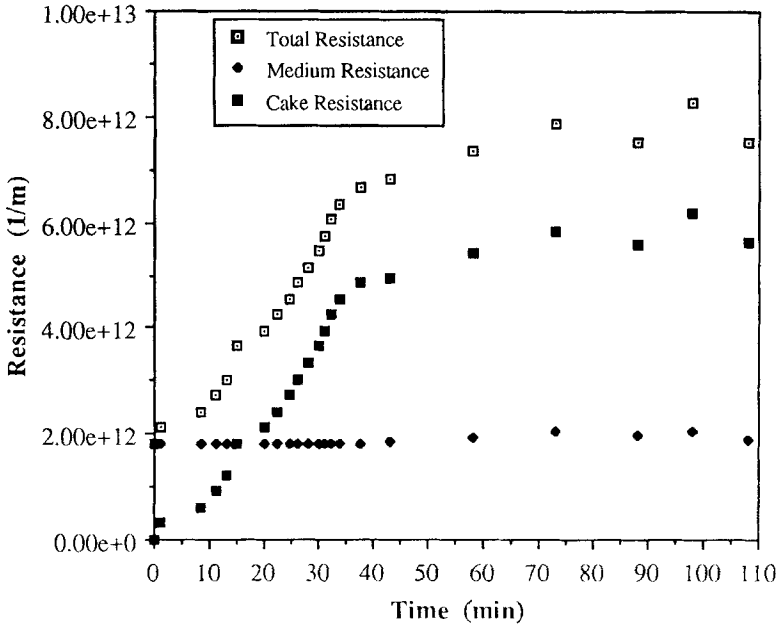

FIGURE 4. Transient medium, cake, and total resistance during the filtration of 10,900 mg/kg sodium nitrate solution (P = 27.6±0.7 MPa; T = 423-438°C).

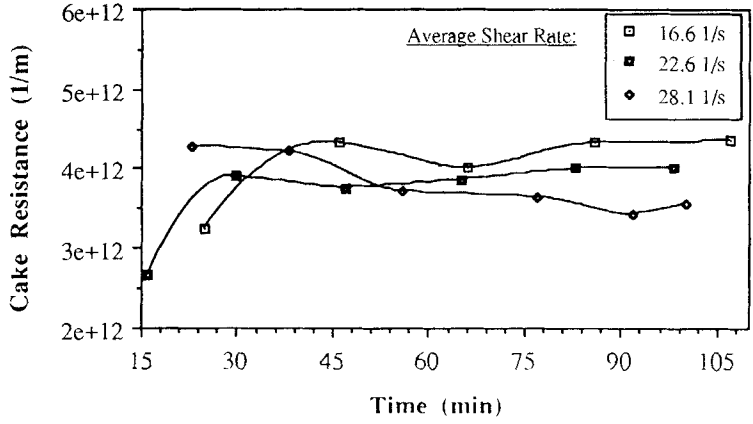

FIGURE 5. Effect of the shear rate on the cake resistance during filtration of a 5,000±250 mg/kg sodium nitrate solution (P = 27.6±0.7 MPa; T = 422-446°C).

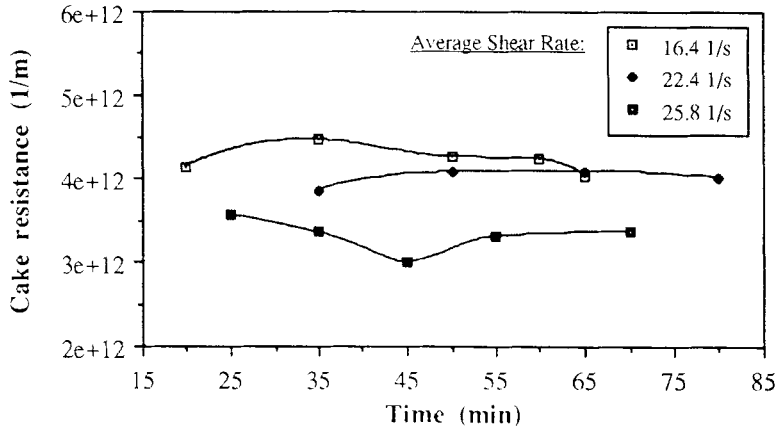

FIGURE 6. Effect of the shear rate on the cake resistance during the filtration of a 21,800±500 mg/kg sodium nitrate solution (P = 27.6±0.7 MPa; T = 384-439°C).

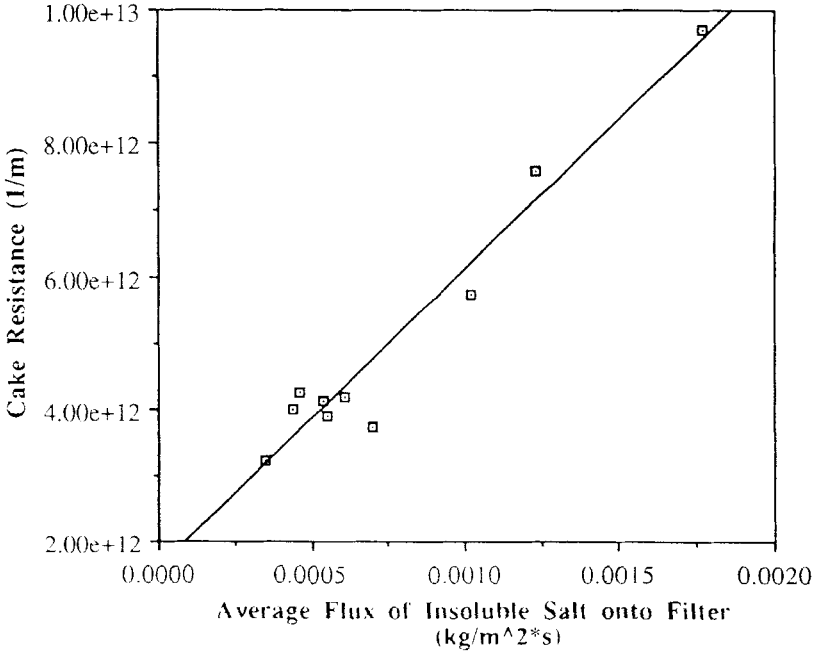

FIGURE 7. Correlation between the insoluble salt flux and the steady state cake resistance (P = 27.6±0.7 MPa; T = 402-446°C)

increased insoluble salt flux was observed for experiments conducted within the same system temperature range (420°C to 450°C). This resulted in an empirical expression for predicting the steady state cake resistance:

$$R_c = 1.581*10^{+12} + 4.507*10^{+15} (J^*_{salt}), \quad (5)$$

with $R^2 = 0.946$, and the p-value for the F-test was 0.0001.

Separation Mechanism of a Molten Salt from SCW

In traditional cross-flow filtration applications, particles are retained by the filter element due to size restrictions while the fluid passes through the filter pores. The separation efficiency is therefore, among others, a function of the particle size distribution. The sum of the hydraulic pressure and the pressure exerted by the particles due to the cumulative drag is balanced by the mechanical strength of the filter element. This reasoning does not hold for separation of sodium nitrate from SCW. Molten salt crystals are deformable and therefore can be forced through the filter membrane by the transmembrane pressure drop. Existing cross-flow filtration models could not be used to model the fluidized cake formation or to calculate the steady state filtrate flux. In all existing models, the particle size of the particles in suspension is used. No good estimate for the "particle size" of the insoluble salt was available. Therefore, different physical mechanisms were needed to explain the observed separation.

The separation efficiency for molten salt from SCW was explained by the different relative permeability (k) of the medium for molten salt and supercritical solution. It was calculated (4) that the criteria for incompressible flow (20) of a compressible fluid (supercritical water) were satisfied and that laminar flow existed in the pores (using the Hagen-Poiseuille law, $5 < Re_{max} < 200$). Therefore, the force balance on a molten salt or SCW particle passing through a filter pore could be written as:

$$F_p - F_c - F_d = 0, \quad (6)$$

where F_p was the pressure force due to the transmembrane pressure drop, F_c the force due to the surface tension of the fluid (= capillary force), and F_d the drag force exerted by the walls of the capillary on the laminar flowing fluid particle.

For a molten salt particle, these forces were defined as:

$$F_p = \Delta P^* \pi^* (0.5^* d_c)^2 , \quad (7)$$

$$F_c = \sigma_s^* \pi^* d_c , \quad (8)$$

$$F_d = 8\pi^* \mu_s^* t_c^* U_{ws} ; \quad (9)$$

where

d_c = diameter of the capillary tube (= pore size) (m),

σ_s = surface tension of the molten salt phase (Nm^{-1}),

μ_s = viscosity of the molten salt phase (Pa.s),

t_c = length of the capillary tube (m), and

U_{ws} = the average salt velocity in the capillary tube (m/s).

A similar set of equations was written for a supercritical solution (SCS) particle. Since the viscosity of SCS was lower than the viscosity of the molten salt phase, the drag force exercised on SCS by the capillary wall was smaller than the drag force on the molten salt. This implied that passage of SCS through the filter required less pressure drop than required for the passage of molten salt.

A suction (= pressure) force was generated by the pressure drop according to Eq. 7. During experiments with low salt fluxes and during the initial stage of the experiments, the fluidized filter cake was prevented from passing through the pores of the filter because the sum of the capillary force and the drag force was bigger than the pressure force. The molten salt particles moved along the filter and were collected in the retentate. However, the pressure drop increased with increased salt flux; this pressure drop eventually provided enough force to overcome the resistance to passage provided by the drag force and the capillary force. The entire pore was filled with molten salt, and the force balance of Eq. 6 reduced to the force balance of laminar flow in a capillary tube $F_p - F_d = 0$.

To calculate the drag force, the average laminar fluid velocity in the capillary tube ("pore velocity") of the molten salt and SCW needs to be calculated. Therefore, the average salt and water velocity in the capillary needs to be coupled with the average molten salt flux (V_{ws}) and supercritical water flux (V_{wf}), respectively. This coupling and the ratio between V_{ws} and V_{wf} can be determined using the standard mathematical expressions for simultaneous flow of two immiscible fluids in porous media (4, 23, 24). Key in these expressions is the relative permeability of the porous medium for each fluid phase.

The calculated values for the salt and SCW solution flux can be used to calculate the concentration of the inorganic salt in the filtrate using:

$$C_{filtr} = \frac{V_{wf}}{V_w} * S + \frac{V_{ws}}{V_w} * C_S \,, \tag{10}$$

with $V_{wf} + V_{ws} = V_w$, C_S the salt concentration of the salt phase in mg/kg, S the salt solubility in mg/kg, and C_{filtr} the filtrate concentration under ambient conditions (mg/kg). For a pure salt phase, $C_S = 10^{+6}$ mg/kg. No data were found in the literature for the salt phase viscosity and surface tension that would have allowed quantification of the described process.

CONCLUSIONS

Cross-flow microfiltration was effective in removing sodium nitrate from supercritical water. Separation efficiencies up to 85% were observed at 27.6 MPa and 470°C. Empirical equations were developed to predict the filtrate concentration and fluidized cake resistance as a function of the salt flux to the filter. The maximum achievable separation efficiency was limited by the salt solubility under the process conditions. No fouling, even at high filtrate to retentate ratios (9:1), of the filter membrane occurred. The viscosity differential between supercritical water and the molten sodium nitrate was likely to be responsible for the observed separation. Corrosion of the filter element was observed; hence, investigation into the use of more corrosion resistant filter materials merits consideration.

ACKNOWLEDGMENTS

Funding for this research was provided by the National Science Foundation under Grant BCS-9112443, the Advanced Research Program of the State of Texas, the Separations Research Program of The University of Texas at Austin, and the Bettie Margaret Smith Chair in Environmental Engineering. This research was made possible by staff and equipment provided by The University of Texas at

Austin and Eco Waste Technologies, Inc., Austin, Texas. The authors would like to thank Dr. Desmond F. Lawler of the University of Texas at Austin, Environmental and Water Resources Engineering Program, and Dr. Frank M. Tiller of the University of Houston, Department of Chemical Engineering for their contributions.

REFERENCES

1. R.K. Helling and J.W. Tester, Environ. Sci. Technol. 22, 1319 (1988).
2. D.S. Lee, L. Li, and E.F. Gloyna, J. Supercrit. Fluids. 3, 249 (1990).
3. J.S. Gallagher and L. Haar, NIST Reference Database 10 (1988).
4. M.G.E. Goemans, L. Li, and E.F. Gloyna, The Separation of Inorganic Salts and Metal Oxides from Supercritical Water by Cross-Flow Microfiltration, Technical Report CRWR 248, Bureau of Engineering Research, The University of Texas at Austin, Austin, Texas, 1994.
5. M. Uematsu and E.U. Franck, J. Phys. Chem. Ref. Data 9, 1291 (1980).
6. J.F. Connolly, J. Chem. Eng. Data 11, 13 (1966).
7. H.A. Pray, C.E. Schweickert, and B.H. Minnich, Ind. Eng. Chem. 44, 1146 (1952).
8. E.U. Franck, J. Sol. Chem. 2, 339 (1973).
9. O.I. Martynova, in High Temperature, High Pressure Electrochemistry in Aqueous Solutions, NACE-4, 1976, p. 131.
10. W.R. Killilea, G.T. Hong, K.C. Swallow, and T.B. Thomason, SAE Technical Paper Ser. No. 881038 (1988).
11. P.C. Dell'Orco, L. Li, and E.F. Gloyna, Sep. Sci. Technol. 28, 625 (1993).
12. F.J. Armellini and J.W. Tester, SAE Technical Paper Ser. No. 901313 (1990).
13. F.J. Armellini and J.W. Tester, Fluid Phase Equilibria 84, 123 (1993).
14. P.C. Dell'Orco, H.K. Eaton, R.T. Reynolds, and S.J. Buelow, The Solubility of 1-1 Electrolytes in Supercritical Water, Report LA-UR-92-3359, U.S. Department of Energy, Los Alamos, New Mexico, 1992.
15. A.L.,Horvath, Handbook of Aqueous Electrolyte Solutions: Physical Properties, Estimation and Correlation Methods, Ellis Horwood Limited, England (1985).

16. M. Cheryan (ed.), Ultrafiltration Handbook, Chapter 4, Technomic Publishing Company, Lancaster, Pennsylvania (1986).

17. J.D. Henry, in Recent Developments in Separation Science, Vol. 2, CRC Press, Inc., Boca Raton, Florida, 1972, p. 205.

18. J. Murkes and C.G. Carlsson, Cross-Flow Filtration, John Wiley & Sons, New York (1988).

19. R. Singh, Chem. Eng. Prog. 6, 59 (1989).

20. C.A. Romero and R.H. Davis, J. Membr. Sci. 62, 249 (1991).

21. V.L. Fowler and J.D. Hewitt, Cross-Flow Filtration of Oak Ridge National Laboratory Liquid Low-Level Waste, Report ORNL/TM 10742, U.S. Department of Energy, Oak Ridge, Tennessee, 1989.

22. R.L. Panton, Incompressible Flow, John Wiley & Sons, New York (1984).

23. J. Bear, Dynamics of Fluids in Porous Media, Chapter 6, Dover Publications, Inc., New York (1972).

24. F.A.L. Dullien, Porous Media, Fluid Transport and Pore Structure, Chapter 9, Academic Press, New York (1979).